Site-Directed Mutagenesis and X-ray Crystallography of the PQQ-Containing Quinoprotein Methanol Dehydrogenase and Its Electron Acceptor, Cytochrome c_L[†,‡]

P. R. Afolabi, F. Mohammed, K. Amaratunga, O. Majekodunmi, S. L. Dales, R. Gill, D. Thompson, J. B. Cooper, S. P. Wood, P. M. Goodwin, and C. Anthony*

Division of Biochemistry and Molecular Biology, School of Biological Sciences, University of Southampton, Southampton SO16 7PX, U.K.

Received December 26, 2000; Revised Manuscript Received May 29, 2001

ABSTRACT: Two proteins specifically involved in methanol oxidation in the methylotrophic bacterium *Methylobacterium extorquens* have been modified by site-directed mutagenesis. Mutation of the proposed active site base (Asp303) to glutamate in methanol dehydrogenase (MDH) gave an active enzyme (D303E-MDH) with a greatly reduced affinity for substrate and with a lower activation energy. Results of kinetic and deuterium isotope studies showed that the essential mechanism in the mutant protein was unchanged, and that the step requiring activation by ammonia remained rate limiting. No spectrally detectable intermediates could be observed during the reaction. The X-ray structure, determined to 3 Å resolution, of D303E-MDH showed that the position and coordination geometry of the Ca^{2+} ion in the active site was altered; the larger Glu303 side chain was coordinated to the Ca^{2+} ion and also hydrogen bonded to the O5 atom of pyrroloquinoline quinone (PQQ). The properties and structure of the D303E-MDH are consistent with the previous proposal that the reaction in MDH is initiated by proton abstraction involving Asp303, and that the mechanism involves a direct hydride transfer reaction. Mutation of the two adjacent cysteine residues that make up the novel disulfide ring in the active site of MDH led to an inactive enzyme, confirming the essential role of this remarkable ring structure. Mutations of cytochrome c_L, which is the electron acceptor from MDH was used to identify Met109 as the sixth ligand to the heme.

Methanol dehydrogenase (MDH)[1] is a soluble quinoprotein, whose prosthetic group is pyrroloquinoline quinone (PQQ). It catalyses the first reaction in an unusual periplasmic electron transport chain responsible for oxidation of methanol to formaldehyde in methylotrophic bacteria (*1*, *2*):

$$\text{MeOH} \rightarrow \text{MDH} \rightarrow \text{cytochrome } c_L \rightarrow \text{cytochrome } c_H \rightarrow \text{oxidase} \rightarrow \text{oxygen}$$

MDH is the first PQQ-containing quinoprotein to have its X-ray structure determined (*3*−*10*), the enzyme from the facultative methylotroph *Methylobacterium extorquens*, the subject of this paper, being determined to 1.94 Å (*9*). MDH has an $\alpha_2\beta_2$ tetrameric structure, each small β-subunit (74 amino acids) folding around the surface of an α-subunit (600 amino acids). The α-subunit is a superbarrel made up of eight radially arranged β-sheets (the "propeller fold"). PQQ, intimately bonded to a Ca^{2+} ion, is buried in the interior of the superbarrel. The floor of the active site chamber is formed by a tryptophan residue and the ceiling formed by a ring structure arising from a disulfide bridge between adjacent cysteine residues joined by a novel nonplanar peptide bond

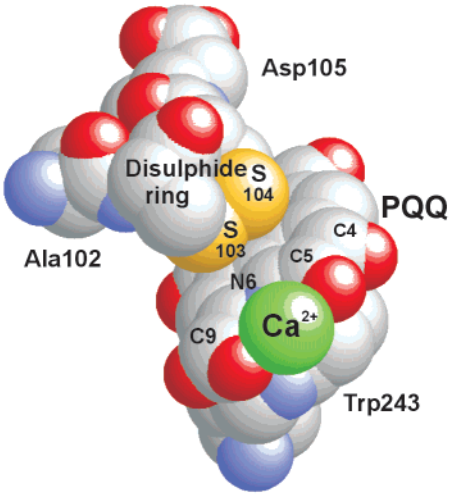

FIGURE 1: Disulfide bridge, PQQ, and Ca^{2+} in the active site of MDH.

(Figure 1). This is the only example of such a structure in an active enzyme; reduction of this bond reversibly inactivates MDH but its specific function is unknown. It is unlikely to be involved directly in electron transfer between $PQQH_2$ and its electron acceptor, and it may a play a role in protecting the intermediate free radical form of the enzyme, which is the form in which MDH is usually isolated (*11*).

MDH catalyses a ping-pong reaction, consistent with reduction of PQQ by methanol and release of formaldehyde, followed by oxidation of $PQQH_2$ back to the quinone by

[†] This work was supported by The Wellcome Trust and BBSRC (U.K.).

[‡] The coordinates of the wild-type MDH and the D303E-MDH have been deposited with the Brookhaven Protein Data Bank (codes 1h4i and 1h4j, respectively).

* To whom correspondence should be addressed.

[1] Abbreviations: MDH, methanol dehydrogenase; PES, phenazine ethosulphate; PQQ, pyrroloquinoline quinone.

10.1021/bi002932l CCC: $20.00
Published on Web 07/26/2001

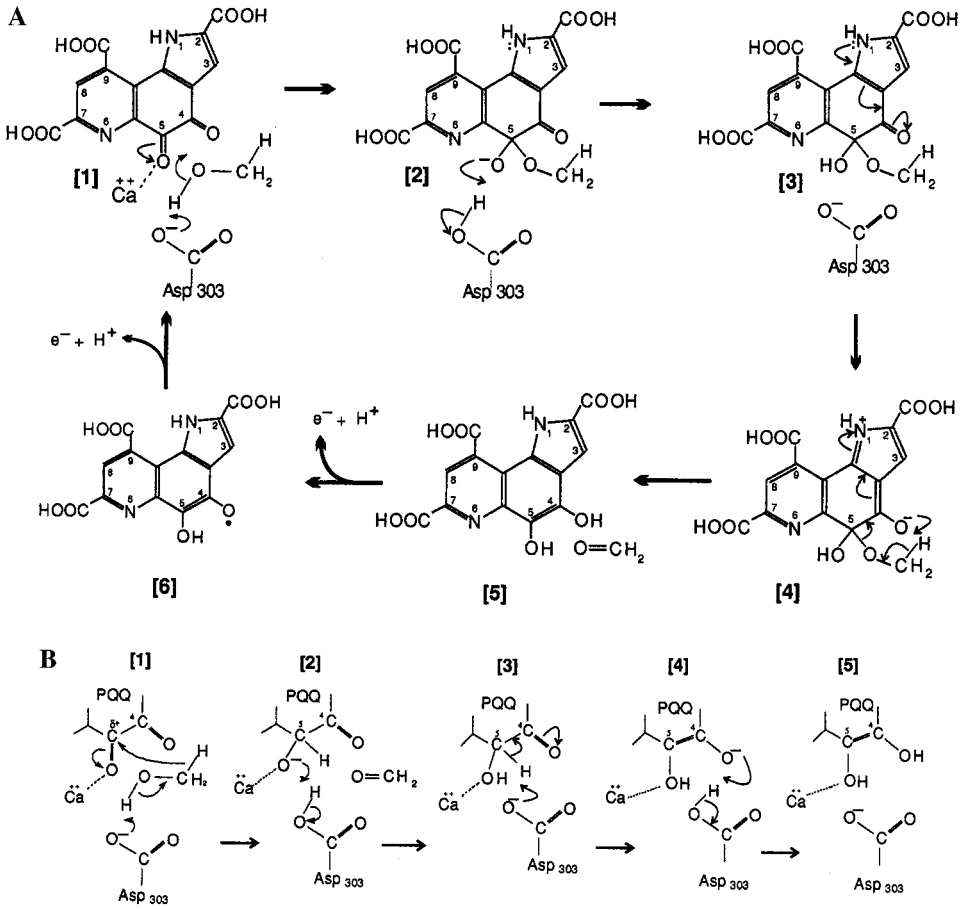

FIGURE 2: Proposed mechanisms for MDH. In both mechanisms the reaction is initiated by proton abstraction. In panel A, there is an addition−elimination reaction involving formation of a covalent hemiketal intermediate, whereas in panel B, there is a concerted hydride transfer. In panel A, the polarization of the C4 carbonyl is facilitated by the ionization of the pyrrole nitrogen. In panel B, the tautomerisation is probably facilitated by the Asp303.

way of the free radical semiquinone (*12*−*14*). It has been proposed that a catalytic base (possibly Asp303) initiates the reaction by abstraction of a proton from the alcohol substrate (Figure 2). The subsequent steps in the mechanism involve formation of a hemiketal intermediate in an addition−elimination reaction (Figure 2A) or a hydride transfer (Figure 2B). The Ca^{2+} ion is coordinated to the carbonyl oxygen (O5) of PQQ, and it has been proposed that this facilitates its polarization and subsequent attack on the electrophilic C5 atom by an oxyanion or hydride (*1*, *2*). Arg331 is within hydrogen bond distance of the O5 carbonyl oxygen and may also contribute to the polarization of C5. Until recently the balance of evidence has appeared to be in favor of the addition−elimination mechanism, but recent work on the structure of the related soluble glucose dehydrogenase (*15*, *16*) has strongly favored the hydride transfer mechanism for that enzyme and it has been argued that a similar mechanism also operates in MDH (*17*).

The physiological electron acceptor for MDH is cytochrome c_L, a large, specific, novel *c*-type cytochrome which only occurs in methylotrophic bacteria (*18*, *19*). Its X-ray structure has not been determined but that of a related cytochrome c_{551i} from *Paracoccus denitrificans* has been published (*20*). Cytochrome c_L is oxidized by cytochrome c_H whose structure has recently been determined and also shown to possess some unusual features (*21*).

Most ideas about the structure and mechanism of PQQ-containing quinoproteins derive from studies of MDH which is therefore the most obvious target for site-directed mutagenesis. This has not been possible previously, however, and the only mutagenesis studies of this type of enzyme have depended on our model structure (based on MDH coordinates) of the structurally homologous membrane glucose dehydrogenase of *Escherichia coli* (*22*−*26*). Mutagenesis of MDH is difficult because more than 30 genes are required for methanol oxidation, including those involved in the biosynthesis of MDH, PQQ, and cytochrome c_L (*27*). The genes encoding the α and β subunits of MDH (*mxaF* and *mxaI*) and cytochrome c_L (*mxaG*) are located on an operon together with *mxaJ* (function unknown). The *mxaFJGI* genes are transcribed from a promoter upstream of *mxaF* and form part of an 11 gene cluster [*mxaFJGIR*(*S*)*ACKLD*], the three genes *mxaAKL* being involved in Ca^{2+} ion insertion (*28*, *29*). These methanol oxidation genes are absent from *E. coli* which is also unable to synthesize PQQ or *c*-type cytochromes. The usual methods for site-directed mutagenesis and protein expression in *E. coli* are therefore not directly applicable and the alternative, of using *M. extorquens* itself, poses its own particular problems. For example, its high G+C ratio limits the number of restrictions sites available for cloning steps (giving large inserts which are unstable in M13 phage), and there are difficulties when inserting small fragments into the large IncPI plasmids which are required for expression of mutant genes in *M. extorquens*.

The present paper describes methods for the production of site-directed mutants in *M. extorquens* which have been

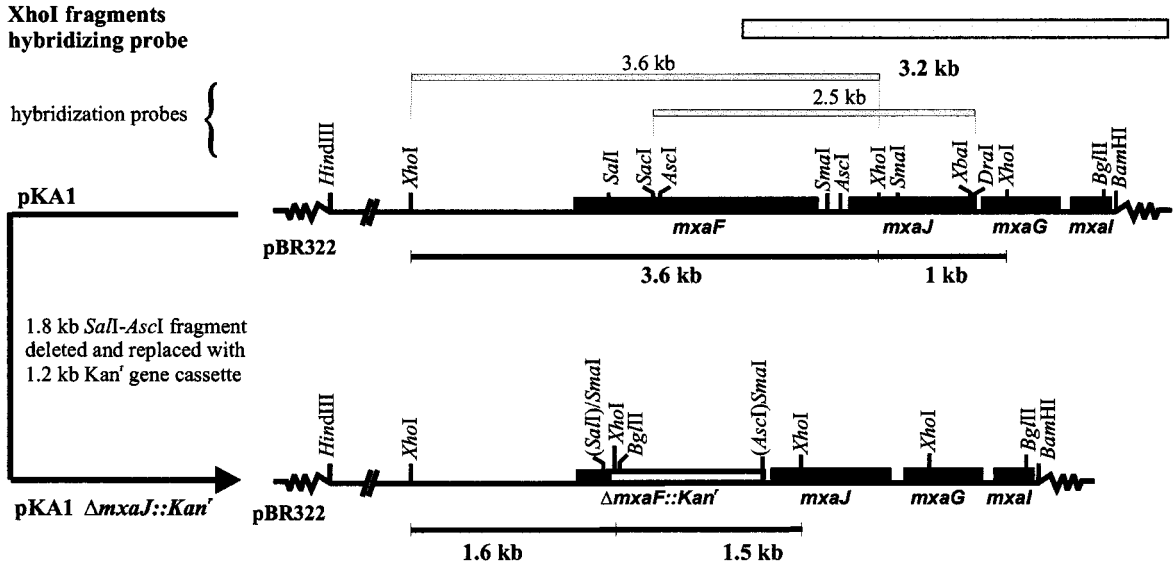

FIGURE 3: Restriction map of the *mxaFJGI* operon in pKA1 and pKA1 (Δ*mxaF::Kan*^{r}). The map is not strictly to scale. Transcription is from left to right. The white box represents the kanamycin resistance reporter gene replacing the deleted DNA. The probe used for Southern hybridization is shown as a gray box.

employed successfully to produce mutations in cytochrome c_L and MDH, to investigate the role of the novel disulfide ring structure in the MDH active site, and, together with X-ray crystallography, to test hypotheses concerning its reaction mechanism.

MATERIALS AND METHODS

General Methods Used in Site-Directed Mutagenesis. Most bacterial strains, plasmids and phage have been described previously (*30*, *31*). All the genes used in this work are depicted on the restriction map of plasmid pKA1 (Figure 3), and the synthetic mutagenic oligonucleotide primers are listed in Figure 4. Restriction enzymes were obtained from Promega or New England Biolabs. Growth of *E. coli*, large scale plasmid preparation by the alkaline lysis method, DNA manipulations, transformation of *E. coli*, and agarose gel electrophoresis are described in (*32*). Purification of *M. extorquens* chromosomal DNA, bacterial matings, Western blotting for identification of MDH and cytochrome c_L, oligonucleotide syntheses and DNA sequencing were carried out as described in (*33*). DNA fragments from agarose gels were purified with a QIAEX II kit (QIAGEN). The Wizard miniprep DNA purification system (Promega) was used for small scale plasmid isolation from *E. coli*. After mutagenesis, *M. extorquens* was propagated on appropriate selection media containing kanamycin and tetracycline. At every stage, mutations were confirmed by restriction analysis and/or DNA sequencing. Further details of procedures are provided in ref *34* (for cytochrome c_L mutations), in ref *33* for disulfide bridge mutations and production of the deletion mutant, and in ref *35* for production of the D303E-mutant.

Production of a Marked Polar Deletion Mutant for MDH Expression. To produce the deletion mutant for MDH expression (Δ*mxaF::Kan*^{r}), a suicide vector (pKA415F) was needed to deliver the *mxaF* deletion into the chromosome of *M. extorquens*. To achieve this a *Sal*I-*Asc*I fragment including *mxaF* was removed from pKA1, creating pKA1Δ*mxaF*; the ligated blunt ends regenerated a *Sal*I site into which a *Sal*I−*Sna*BI adaptor was inserted (Figure 4).

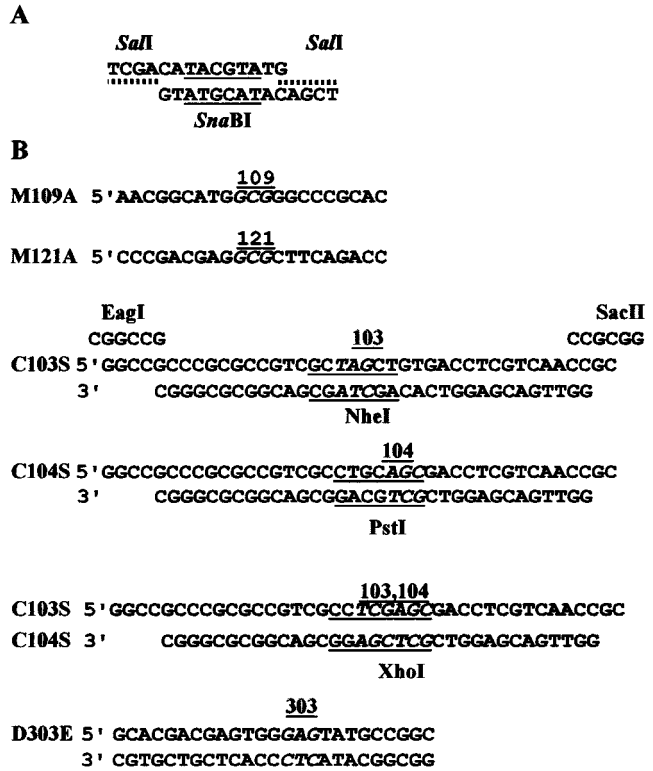

FIGURE 4: Synthetic oligonucleotides used for site directed mutagenesis. (A) Introduction of the *Sal*I/*Sna*I adaptor in production of the deletion mutant. (B) production of mutations in structural genes for cytochrome c_L (M109A, M121A) and MDH (C103S, C104S, C103S/C104S, and D303E). The mutated nucleotides are in italics; the positions of new restriction sites created by the mutation are indicated by underlining.

The 1.2 kb *Sma*I fragment carrying the kanamycin resistance gene from pUC4−KIXX (*33*) was cloned into the *Sna*BI site which, like *Sma*I, generated blunt ended DNA fragments. The *Sal*I−*Sna*BI adaptor was used after several unsuccessful attempts to clone the kanamycin resistance marker directly into the filled-in *Sal*I and *Asc*I sites (within *mxaF*); use of the adaptor also circumvented the screening that would have been required after direct cloning in order to avoid clones

with a 0.4 kb *Sal*I−*Asc*I deletion or a 1.4 kb *Asc*I−*Asc*I deletion resulting from the presence of two *Asc*I sites within *mxaF*. The orientation of the *kan*^{r} marker gene was determined by restriction analysis of plasmid DNA using the *Bgl*II site at one end of the insert, to select a clone carrying the kanamycin resistance gene in the "forward" orientation (in relation to *mxaFJGI*). All subsequent steps were performed as described for a *mxaJ* deletion mutant (*28*, *29*). The required mutant, produced by a double-crossover event after introduction of pKA415F into *M. extorquens*, was confirmed by hybridization analysis using the wild-type 3.6 kb *Xho*I fragment containing *mxaF* and part of the *mxaJ* sequence from pKA1 as a probe (Figure 3).

The deletion mutant (Δ*mxaF::Kan*^{r}) was unable to grow on methanol but grew normally on methylamine, succinate, pyruvate or β-hydroxybutyrate. It was complemented by pRK310(*mxaFJGI*) (*30*, *31*), allowing growth on methanol. The α-subunit of MDH was absent from sonic extracts which showed no dye-linked MDH activity. The *mxaG* gene product, cytochrome c_L, was expressed, confirming transcription of genes downstream of the kanamycin resistance marker. However, the β-subunit of MDH which is encoded by *mxaI* immediately downstream of *mxaG*, could not be detected by Western blotting. It is possible that the very small β-subunit (8.5 kDa) is unstable in the absence of the α-subunit. This does not cause difficulty because during complementation of the MxaF mutant with the wild-type or mutant pRK310(*mxaFJGI*), the gene encoding the small β-subunit (*mxaI*) is also present.

Site-Directed Mutants of MDH. Mutagenesis of the altered disulfide bridge depended on in vitro synthesis of double stranded mutant DNA (Figure 4). The 342 bp *Sal*I−*Sac*I fragment containing the Cys 103/104 region of *mxaF* was cloned from pKA1 into M13mp18 (giving M13KAO). A double-stranded, 40 bp, *Eag*I−*Sac*II fragment within the *Sal*I−*Sac*I insert of M13KA0 was replaced by mutated *Sal*I−*Sac*I fragments (Figure 4), constructed in vitro by annealing two complementary oligonucleotides with *Eag*I and *Sac*II cohesive ends incorporated at either end. The mutation was introduced via a *Sal*I−*Sna*BI adaptor and the 342 bp fragment cloned back into pKA1. The restriction sites introduced with each mutation (Figure 4) were also designed to aid screening of mutant clones in subsequent steps (*33*).

Mutagenesis of the proposed active-site base to give the D303E-MDH was carried out using the Stratagene Quik-Change system. A 2.83kb *Sal*I−*Xba*I fragment containing part of *mxaF* and all of *mxaJ* was cloned into pBluescript^{R}II KS, chosen because it is not supercoiled and it is very small (2.96 kb), thus providing the template for the mutagenic reaction. The mutated DNA was excised using *Asc*I, and the 1.36kb fragment cloned into pKA1 and and the complete operon carrying the D303E mutation in *mxaF* was then cloned from pKA1 into pRK310 (*35*).

Site-Directed Mutagenesis of Cytochrome c_L (encoded by mxaG). The *mxaGI* genes were cloned (using *Xba*I and *Bam*HI) into pM13mp18 for mutagenesis (Figure 4) by the Kunkel method (*36*, *37*); the single-stranded pM13GI DNA was used as a template for second strand production in vitro using T4 DNA polymerase, the mutant DNA being subsequently cloned into the intermediate vector pKA1 (*33*, *34*).

Characterization of Proteins. M. extorquens was grown on methanol media or on methylamine with methanol added to induce synthesis of MDH and cytochrome c_L; methods used for growth, harvesting, preparation of extracts, purification and assay of cytochromes and methanol dehydrogenase (using the artificial electron acceptor phenazine ethosulophate, PES) are described in refs *38* and *39*. UV−vis and CD spectroscopy, methods for determination of thiol groups, and carboxymethylation procedures are described in ref *11*. The production of oxidized enzyme with Wurster's Blue, and its subsequent reduction, is as described in ref *40*. Kinetic investigations, determination of deuterium isotope effects and activation energies were all done using the dye-linked assay system as described in ref *40*; during measurements of ammonia activation on the deuterium isotope effect, the concentration of methanol (800 mM) was sufficient to give about 90% of the V_{max} value. Binding energies were calculated from the measured K_m values for methanol.

Determination of the Structure of D303E-MDH. Crystals were grown in the absence of methanol using the hanging drop/vapor diffusion method as described previously for WT-MDH (*41*). The well solution (1 mL) contained 14.5% poly(ethylene glycol) (6000), 20 mM Tris-HCl buffer (pH 9.5) and 10 mM $CaCl_2$. The hanging drops contained equal volumes of this solution and MDH (20 mg/mL in 5 mM Tris buffer, pH 9.2). Crystals (1.0 × 0.2 × 0.1 mm) were obtained after incubation in the dark for 1 month at 4 °C. X-ray data from a wet-mounted D303E-MDH crystal were collected in house using a 30 cm Mar-Research imaging plate detector system. The X-ray source was an ENRAF NONIUS FR591 rotating anode generator operated at 50 kV and 100 mA, producing CuKα radiation via a graphite monochromator. A total of 180 images, each covering an oscillation angle of 1°, was recorded with an exposure time of 20 min per frame and a crystal-to-detector distance of 230 mm. Intensity data were processed with MOSFLM (*42*) and scaled and merged using programs of the CCP4 suite (*43*).

The crystals were estimated to have a solvent content of 44% (*44*), assuming that there are two $\alpha_2\beta_2$ tetramers in the asymmetric unit. Initial phases were obtained by the molecular replacement method with MOLREP (*45*), using an $\alpha_2\beta_2$ tetramer of wild-type MDH as the search model (*9*). Reflections in the 20−3.0 Å resolution range were used in the cross rotation calculations, with a range of integration radii values (30−70 Å). The cross rotation function calculated with a radius of 55 Å yielded two significant cross-rotation peaks at 12.6 and 10.7σ, thus confirming the presence of two $\alpha_2\beta_2$ tetramers within the asymmetric unit. The highest cross rotation function solution yielded a significant translation function peak at 25σ, with the next peak being at 5σ. This solution was fixed and the translation function was repeated to determine the relative position of the second $\alpha_2\beta_2$ tetramer, yielding the highest peak at 27 σ (the next peak being at 13σ). Following the positioning of both $\alpha_2\beta_2$ tetramers in the target asymmetric unit, the crystal packing of this solution was viewed using MOLPACK (*46*) to verify sensible crystal contacts. Refinement of the molecular model was performed with the program CNS (*47*); the progress of refinement was monitored by setting aside 5% of the reflections for free *R*-factor (R_{free}) calculations (*48*). Initially, the model was subjected to 20 cycles of rigid body refinement, which reduced the *R*-factor from 45.7% (R_{free} = 42.5%) to 24.7% (R_{free} = 24.9%). The refined model was used to calculate σA-weighted electron density maps that

were subjected to 4-fold noncrystallographic symmetry (NCS) averaging. All map inspections and model manipulations were performed with the program QUANTA (Molecular Simulations Inc., Burlington, Massachusetts). Initial examination of the averaged maps revealed difference density for one PQQ molecule, one Ca^{2+} ion and a Glu303 side chain in each α subunit, thus providing support for the chosen molecular replacement solution. Further refinement was carried out at 3 Å using the CNS simulated annealing protocol (torsion-angle) during which the model was raised to 2500 K and then slowly cooled to 300 K in 25 K decrements. Throughout refinement, NCS restraints were maintained since their release did not lower the R_{free} value. Alternating cycles of model building and refinement resulted in convergence (R-factor = 18.7%, R_{free} = 21.7%). The final model was analyzed with PROCHECK (*49*), and displayed acceptable geometry for both main chain and side chain parameters. Inspection of the Ramachandran plot indicated that 82.6% of the amino acid residues are in the "most favored" regions, 16.5% are in "additionally allowed" regions, 0.2% are in "generously allowed" regions and 0.7% in "disallowed" regions. The "disallowed" residues in each $\alpha\beta$ subunit (Lys19, Asn52, Asp105, and Lys166) were well-defined by electron density.

RESULTS

Site-Directed Mutagenesis in M. extorquens. The starting point for mutagenesis was the 8.6 kb *Hin*dIII fragment containing the *mxaFJGI* operon, cloned previously into the broad host-range vector pVK100, able to replicate in *M. extorquens* (*30*, *31*). All mutagenic programs required a small intermediate vector, pKA1 (total size, about 10 kb) which we have developed specifically for recombinant DNA manipulations using the genome of the methylotroph *M. extorquens*; it is a modified pBR322 plasmid with the Tet^r and *Sal*I sites removed, and the *Hin*dIII−*Bam*HI *mxaFJGI* fragment (6.8 kb) inserted (Figure 3) (*28*, *29*). For expression in *M. extorquens*, mutated genes were transferred from pKA1 to pVK310*mxaFJGI*, thence into a $MxaG^-$ mutant (*30*, *31*) for mutated cytochromes, or into the deletion mutant Δ*mxaF::Kan*^{r} for expression of mutated MDH.

Site-Directed Mutagenesis and Characterization of Cytochrome c_L. Cytochrome c_L is the specific electron acceptor for MDH, and its X-ray structure is being determined as part of a program aimed at elucidating its interaction with MDH, and determining paths of electron transfer to its heme from the PQQ prosthetic group of MDH. Cytochrome c_L is similar in many properties to Class I cytochromes *c* but its amino acid sequence shows that it constitutes a separate novel class of *c*-type cytochromes. A diagnostic characteristic of a typical Class I cytochrome is the position of the methionine that forms the sixth ligand to the heme; this is usually about 60 residues toward the C terminal after the histidine that provides the fifth heme ligand. In cytochrome c_L all three methionines are closer than this and the sequences around the methionines bear no relationship to those around methionine in other *c*-type cytochromes. This work was undertaken to establish an appropriate method of site-directed mutagenesis and expression (see Materials and Methods) for future studies with this cytochrome (cytochrome *c* cannot be mutated and expressed in *E. coli*) and to determine which of the three methionine residues provides the sixth heme ligand. The two methionines mutated to alanine in this investigation were Met109 and Met121 which are conserved in the related cytochrome c_{551i} which has 52% identity of sequence to cytochrome c_L (*18*).

Mutant M121A was able to oxidize and grow on methanol as its sole source of carbon and energy but mutant M109A was unable to do so, indicating that Met109 is possibly the sixth heme ligand. Normal amounts of cytochrome c_L were produced in both mutants and they were purified as described for the cytochrome from wild-type bacteria (*38*, *39*). The UV−vis part of the absorption spectra (240−600 nm) of the dithionite-reduced, and persulfate-oxidized mutant cytochromes were unchanged, showing that no major perturbation of the heme had occurred in either of the two mutant cytochromes. In the oxidized M121A cytochrome c_L, the near-infrared band (695 nm) was also present as normal, showing that the methionine-iron bond remained intact. This cytochrome had also retained its ability to act as electron acceptor for methanol dehydrogenase, the rate of reduction and apparent affinity for the enzyme (K_d, 3 μM) being unchanged.

By contrast, M109A cytochrome c_L was no longer able to act as an electron acceptor for MDH, and the near-infrared band was absent, indicating that the methionine ligand to the heme was lost. The work presented here confirms that Met109 is the sixth ligand to the heme iron in cytochrome c_L and that this is essential for its electron-transfer interactions with MDH. The unchanged spectrum between 500 and 600 nm in the mutant cytochrome indicates that the Met109 ligand had been replaced by an alternative low spin ligand (probably lysine or histidine), while the lack of absorption at 695 nm shows that this ligand is not the adjacent Met108.

During this work it was noticed that, by contrast with the great majority of soluble *c*-type cytochromes, in addition to those cysteine residues which are attached to the heme (*50*), cytochrome c_L has two cysteine residues (C53 and C167), which are not conserved in cytochrome c_{551i}. These "extra" residues could not be carboxymethylated with ^{14}IAA using native or denatured cytochrome c_L. However, after denaturation of the cytochrome followed by reduction with dithiothreitol, both cysteines could be carboxymethylated, suggesting that the cytochrome c_L of *M. extorquens* is unique in having a disulfide bridge in its structure, perhaps conferring greater stability on this large periplasmic cytochrome.

Site-Directed Mutagenesis and Preliminary Characterization of MDH with an Altered Disulfide Bridge in the Active Site. MDH contains a remarkable ring structure, made up of adjacent cysteine residues (Cys103 and Cys104), which lie immediately above the PQQ (Figure 1); this type of structure is not seen in the active site of any other type of enzyme, indicating that it is likely to have some specific function in the PQQ-containing alcohol dehydrogenases which may or may not involve reductive cleavage to the free cysteine residues. To investigate whether it is an essential feature of the active site of MDH both cysteines were mutated to serine (separately and together).

All three mutants (C103S, C104S, C103S/C104S) were unable to oxidize methanol or to use it as their sole source of carbon and energy, although oxidation and growth on other substrates was unchanged. Cytochrome c_L was expressed in all three mutants, as expected, confirming that the mutation had not prevented expression of downstream genes. MDH

Table 1: Kinetic and Thermodynamic Constants for D303E-MDH and WT-MDH

	WT-MDH[a]	D303E-MDH
K_m for methanol (with 15 mM NH_4Cl)	0.003 mM	250 mM
K_a for NH_4Cl (with 800 mM methanol)	2 mM	1.1 mM
K_a for NH_4Cl (with 800 mM deuterated methanol)	7 mM	2.15 mM
deuterium isotope effect (with 20 mM NH_4Cl)	1.6	5.9
deuterium isotope effect (with 1 mM NH_4Cl)	4.3	8.4
activation energy	35.4 kJ/mol	20.2 kJ/mol

[a] Values for WT-MDH are taken from ref *40*.

was synthesized by all three mutants, although at very low levels and the enzymes were completely inactive. These results confirm that the complete disulfide bridge is required for activity, and they are consistent with the previous observation that chemical reduction, to give the reduced thiols, leads to inactive enzyme (*11*). Unfortunately, the very low levels of expression of the mutant protein precluded further investigations, but overexpression of the mutant proteins in an alternative strain should provide sufficient material for further study of this intriguing structure.

Site-Directed Mutagenesis of the Proposed Active Site Base, Asp303, to Glutamate. Initiation of the MDH reaction has been proposed to involve the active site base Asp303; to test this hypothesis Asp303 was mutated to glutamate as described in the Materials and Methods. The growth on 0.5% methanol in batch culture of the D303E mutant was similar to the wild-type strain and the D303E-MDH was produced at wild-type levels; it was purified by the normal procedures, characterized biochemically, and its X-ray structure determined. The main kinetic differences are summarized in Table 1.

Kinetic Analysis of D303E-MDH. Although cytochrome c_L is the physiological electron acceptor during oxidation of $PQQH_2$, most studies of the enzyme and its mechanism have used phenazine ethosulfate (or Wurster's Blue) in the enzyme assay. In this system, there is an absolute requirement for ammonia (or methylamine) as an activator. It is not known what role it plays in the mechanism but deuterium isotope studies (see below) have indicated that it acts in the rate-limiting step of removal of hydrogen from the methyl group of methanol.

In the PES-linked assay, the V_{max} value for purified D303E-MDH (1.29 μmol min^{-1} mg^{-1}) was about 60% higher than that for WT-MDH but the K_m value was increased more than 80000-fold (3 μM to 250 mM). This did not prevent growth in batch culture containing high concentrations of methanol. A large increase in the K_m value was also seen for oxidation of ethanol (60 μM increased to about 1.3 M) and for *n*-propanol (60 μM increased to about 2.2 M). This decrease in apparent affinity for substrate was even greater than that previously observed in MDH containing Ba^{2+} instead of Ca^{2+} in the active site (for Ba-MDH, K_m= 3.5 mM) (*40*).

MDH has an absolute dependence on ammonia as activator in the PES-linked assay system, its main effect being to increase the V_{max} value (*1*, *2*, *40*). This was not changed by the mutation. The K_a of D303E-MDH was slightly decreased (from 2 to 1.1 mM) and very high concentrations were inhibitory (K_i, 70 mM for WT-MDH; 105 mM for D303E-MDH). As previously shown for WT-MDH, the apparent affinity of D303E-MDH for methanol decreased with increasing concentration of activator (Figure 5), the steady state kinetics being consistent with the scheme in Figure 6 which shows that, although methanol and ammonia are both essential for activity, each appears to bind more strongly to the enzyme in the absence of the other. This suggests that substrate and activator sites are not identical but able to interact with each other as previously suggested for WT-MDH (*13*, *52*) and Ba-MDH (*40*). The value of K'_s/K_s (7.2) is a measure of this negative effect of ammonia on the affinity for methanol and K'_a/K_a (numerically the same) reflects the negative effect of methanol on ammonia binding (Figure 6).

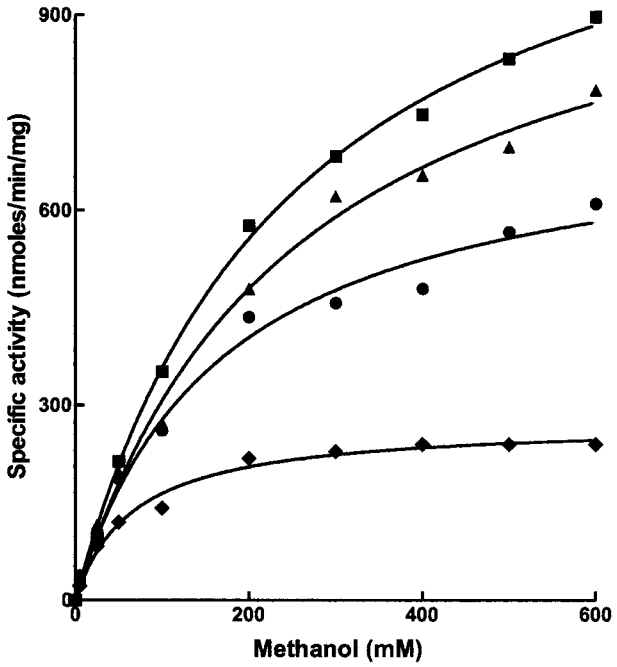

FIGURE 5: Effect of the concentration of ammonia and methanol on the activity of D303E-MDH in the PES-linked assay system. (■) 15 mM NH_4Cl; (▲) 2.5 mM NH_4Cl; (●) 1.0 mM NH_4Cl; (◆) 0.25 mM NH_4Cl.

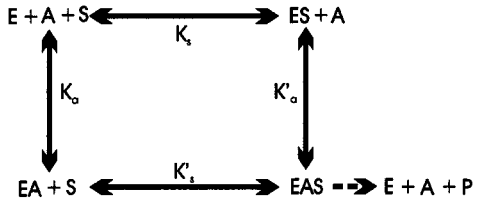

FIGURE 6: Kinetic scheme for the activation of D303E-MDH by ammonia. This scheme shows that the combination of enzyme (E) with substrate (S) is dependent on the activator ammonia (A); thus, E and EA have different affinities for the substrate. The equation for this scheme is $v = V_{max}/(1 + K'_s/S)\ \{1 + K_a/A\ (1 + S/K_s)/(1 + S/K'_s)\}$. When the measured reaction rates were fitted to this equation, the values of the constants were shown to be as follows: K_a = 0.15 mM; K'_a = 1.1 mM; K_s = 44.3 mM; K'_s = 321mM (NB: these values are for the dissociation of the complexes).

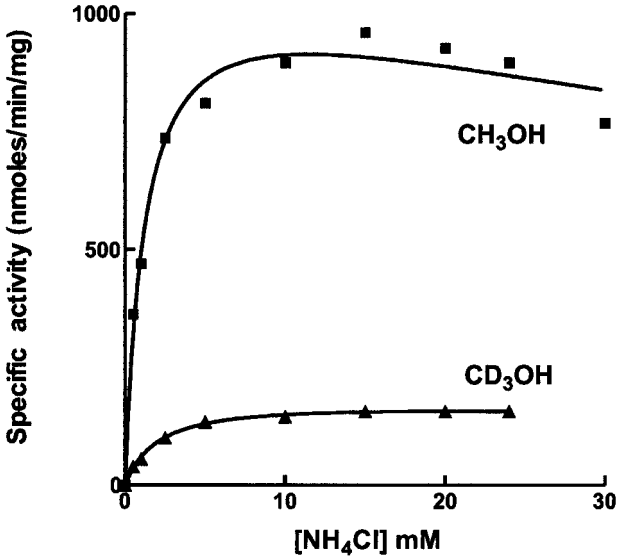

FIGURE 7: Effect of ammonia concentration on the activity of D303E-MDH measured with methanol and deuterated methanol. The effect of NH_4Cl concentration was measured in the PES-linked assay system with high concentrations of substrate (800 mM). The curves were the best fit for the equation $v = V_{max}$ [A]/(K_a + [A])(1 + [A]/K_i), where [A] is the concentration of NH_4Cl.

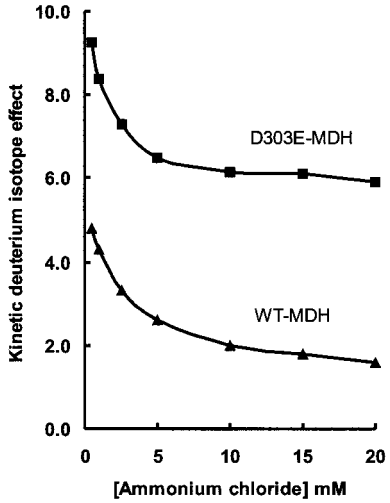

FIGURE 8: Effect of ammonia concentration on the kinetic isotope effect with WT-MDH and D303E-MDH. The values for D303E-MDH were derived from the data in Figure 7 and the values for WT-MDH were taken from ref *40*.

Deuterium Isotope Effect in D303E-MDH. The apparent affinity of D303E-MDH for methanol and deuterated methanol was almost the same (K_m values, 250 and 193 mM, respectively). By contrast, the V_{max} was decreased at least 6-fold with deuterated methanol (Figure 7). The apparent affinity for the activator ammonia was slightly lower with deuterated methanol (K_a, 2.15 mM) than with methanol (K_a, 1.25 mM) (Figure 7); the isotope effect was therefore dependent on the concentration of ammonia, being higher at lower ammonia concentrations, as seen previously with MDH from *Hyphomicrobium* X (*13*) and with Ba-MDH (*40*) (Figures 7 and 8; Table 1). This deuterium isotope effect was greater for D303E-MDH (6 with 20 mM NH_4Cl) than that observed with WT-MDH (1.6 with 20 mM NH_4Cl) but considerably less than the isotope effect (8.0 with 20 mM NH_4Cl) measured with Ba-MDH (*40*). The steps in the mechanism that are affected by the change from protiated substrate to deuterated substrate must be those involving removal of the methyl hydrogen as shown in Figure 2. These are conversion of 4 into 5 in panel A and the conversion of 1 into 2 in panel B. These results exclude the possibility that ammonia activates MDH by encouraging the initial binding of substrate or by affecting the formation of any PQQ-methanol adduct, or by stimulating the reoxidation of reduced PQQ; they confirm the previous proposal that ammonia activates the reduction of PQQ by substrate (*13*, *40*).

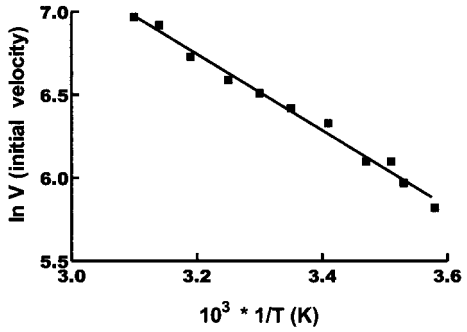

FIGURE 9: Determination of the activation energy for D303E-MDH. Activity of D303E-MDH (6.7 μM) was measured in the PES-linked system with high concentrations of methanol (800 mM) and NH_4Cl (15 mM) at temperatures between 6 °C and 50 °C. The activation energy E_A was calculated from the slope of the best fit line based on the equation $v = A \exp(-E_A/RT)$.

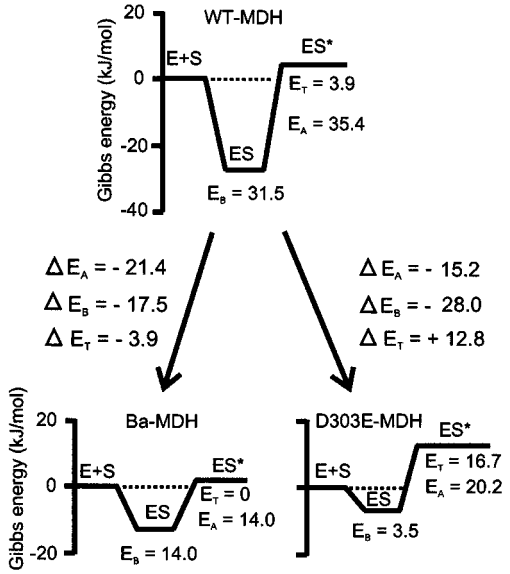

FIGURE 10: Schematic Gibbs free energy changes (in kJ/mol) for the formation of the transition state complex during the activity of methanol dehydrogenase. The changes in Gibbs energies are for the concentrations used in the experiments and not the standard states of 1 M. The values for WT-MDH and Ba^{2+}-MDH are taken from (*40*). E represents the enzyme, S is the substrate, ES is the enzyme substrate complex and ES* is the transition state complex. E_A and E_B represent activation and binding energies, and E_T gives a measure of the energy of the transition state complex. ΔE_A, ΔE_B, and ΔE_T are the differences in these energies occurring when the WT-MDH is changed to Ba^{2+}-MDH and D303E-MDH.

Activation Energy for Methanol Oxidation by D303E-MDH. The activation energy for methanol oxidation catalyzed by D303E-MDH, measured between 6 and 50 °C, was 20.2 kJ/mol (Figure 9) compared with 35.4 kJ/mol for WT-MDH, consistent with the 60% increase in the measured V_{max} value. This decrease in activation energy (15.2 kJ/mol)

Table 2: Data Processing and Refinement Statistics for the D303E-MDH Structure

total number of reflections	134 792
no. of unique reflections	48 502
resolution (Å)	3.0
completeness (%) (highest resolution shell)	91.5 (81.4)
R_{merge} (%) (highest resolution shell)	9.4 (26.5)
multiplicity (highest resolution shell)	3.0 (2.8)
avg $I/\sigma I$) (highest resolution shell)	6.9 (2.6)
resolution range (Å)	30−3
R-factor (%)	18.7
R-free (%)	21.7
no. of reflections in working set	45 246
no. of reflections in test set	2385
no. of protein atoms	20 548
rms bond length deviation (Å)	0.007
rms bond angle deviation (Å)	1.4

occurred concomitantly with an increase of more 80 000 in the K_m for methanol. Assuming that this reflects a change in K_d for methanol then this indicates a decrease in binding energy of 28 kJ/mol. This suggests that in D303E-MDH there must be a decrease in stability of both the transition state complex and the enzyme substrate complex (Figure 10). This finding contrasts with the effect of replacing Ca^{2+} with Ba^{2+} in Ba-MDH where the change in activation energy was almost entirely due to the decrease in stability of the enzyme substrate complex, with little affect on stability of the transition state complex (*40*).

Production of the oxidized form of D303E-MDH and its reduction by methanol. The absorption spectrum of reduced MDH has a peak at 345 nm and a shoulder at 400 nm, which has been ascribed to $PQQH_2$, and the spectrum of the enzyme containing the semiquinone form of PQQ is almost identical; on oxidation, the absorption at 345 nm decreases and the absorption at 400 nm increases (*1*, *2*). The absorption spectrum of D303E-MDH, and the CD spectra (240−400 nm) were shown to be the same as those of WT-MDH in which the PQQ is in either the semiquinone or reduced form, indicating that the secondary structure and the redox state and conformation of PQQ has not been markedly altered by mutation of Asp303 to glutamate.

Spectrophotometric analysis of the mechanism of MDH has been hindered by the difficulty of obtaining a stable oxidized form of the enzyme. When it is produced from the isolated semiquinone form by oxidation with Wurster's blue, MDH becomes very rapidly reduced by the small amounts of endogenous substrate for which the enzyme has an extremely high affinity (*1*, *2*, *40*). By contrast, because of its very low affinity for all substrates, a stable oxidized form of D303E-MDH could be produced readily by incubation with Wurster's blue, and its subsequent reduction measured by the increase in absorption at 345 nm and the accompanying decrease at 400 nm. As expected, the rates of reaction measured in the absence of added substrate and activator (ammonia) were very low, with complete reduction occurring after 12 h. By contrast, when both methanol and ammonia were present, the rate was too fast to measure using conventional spectrophotometry (complete reduction within 2 s). When either ammonia or methanol were added to the oxidized enzyme separately, the rates were sufficiently low to be measured and were identical at the two wavelengths (345 and 400 nm). The first-order rate constants were 4.5×10^{-3} s^{-1} for reduction by endogenous substrate in the presence of ammonia activator, and 1.8×10^{-3} s^{-1} with added methanol in the absence of ammonia. The spectra were identical during both reduction processes, with an isosbestic point at 360 nm and were indistinguishable from those previously published for Ba-MDH (*40*). All the results suggest that only the fully oxidized and fully reduced forms of MDH were present during the reaction. There was no indication of any intermediate form as might have been expected if a methanol or ammonia covalent adduct is an intermediate. If the mechanism does involve such an intermediate, then its spectrum must be very similar to either the oxidized or the reduced forms, or the population of the enzyme in the intermediate state is too small to detect. The D303E-MDH will be used in future studies using stopped flow analysis in order to investigate this further; this approach has been successful in demonstrating the absence of a covalent adduct intermediate in the mechanism of the related

Table 3: Interatomic Distances (in Å) between Key Features in the Active Site of MDH from *Methylobacterium extorquens*

atom 1	atom 2	wild-type MDH; values in parentheses are for MDH from *Methylophilus methylotrophus* (*4*−*6*)	D303E-MDH
Asp303 OD1(OE1 of Glu303)	Ca^{2+}	3.5 (3.2)	2.4
	PQQ O4	6.1 (6.1)	5.1
	PQQ O5	4.1 (4.2)	2.8
	PQQ C5	5.3 (5.4)	4.0
	Arg 331 NH2	3.6 (3.7)	3.6
	Asn261 ND2	3.2 (3.3)	3.8
	Asn 261 OD1	3.5 (3.6)	3.3
Asp303 OD2 (OE2 of Glu303)	Ca^{2+}	4.6 (4.2)	4.3
	PQQ O4	5.2 (5.1)	5.0
	PQQ O5	3.8 (4.1)	3.5
	PQQ C5	5.0 (4.9)	4.7
	Arg331 NH1	5.2 (5.3)	5.7
	Arg331 NH2	3.0 (3.1)	3.5
	Asn261 ND2	5.3 (5.1)	5.5
	Asn261 OD1	5.4 (5.5)	5.4
Arg331 NH1	PQQ O4	2.7 (3.1)	3.0
	PQQ O5	3.4 (3.3)	3.8
	PQ C5	3.7 (4.2)	3.9
Arg331 NH2	PQQ O4	3.3 (3.2)	3.1
	PQQ O5	2.9 (3.0)	2.9
	PQQ C5	3.9 (4.0)	3.7

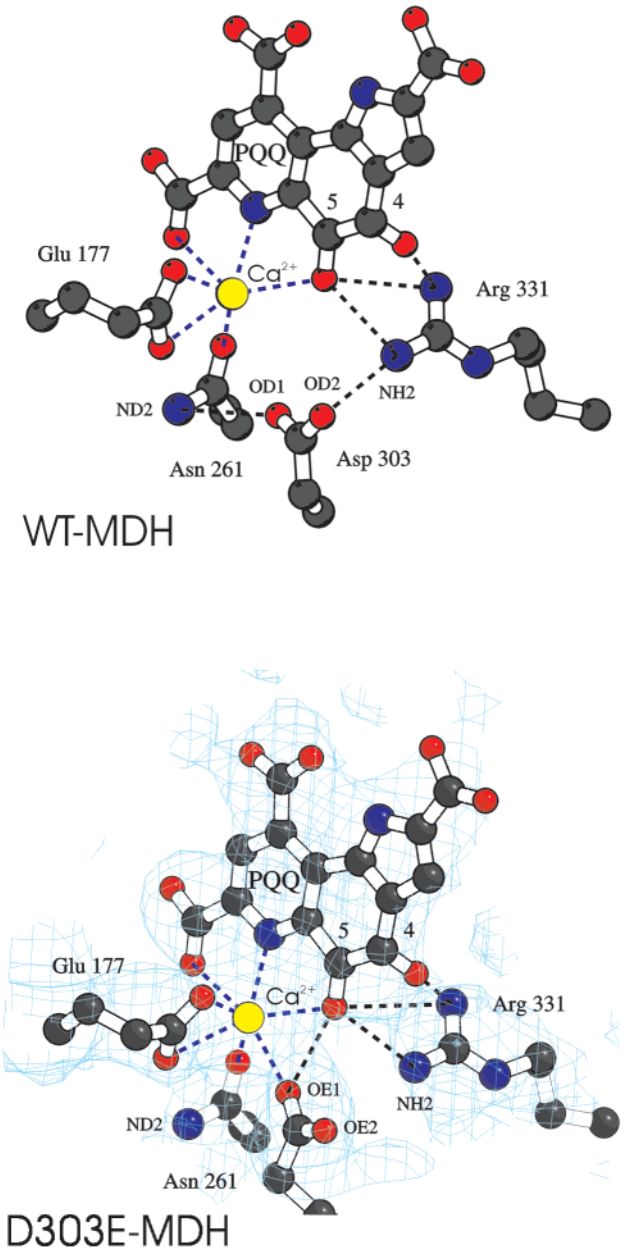

FIGURE 11: Active site of wild-type MDH and D303E-MDH. Key differences are the heptacoordinate Ca^{2+} in the D303E-MDH due to a new coordination to the carboxyl of the Glu303; formation of a new hydrogen bond between OE1 of Glu303 and the O5 of PQQ; and the eradication of bonding of this carboxylate with Asn261 and Arg331. The electron density for the active site residues, PQQ and Ca^{2+} in D303E-MDH are contoured at 1.0 rms.

soluble glucose dehydrogenase of *Acinetobacter calcoaceticus* (*16*).

Structure of D303E-MDH. The two crystal forms of MDH previously used in the structure determination of MDH from *Methylophilus methylotrophus* were both $P2_1$, with a single $\alpha_2\beta_2$ tetramer occupying the asymmetric unit in both crystal forms (*5*). Three types of crystal have previously been obtained for WT-MDH from *M. extorquens*, two of which were used during the initial structure determination, one being orthorhombic ($P2_12_12_1$) and the other triclinic ($P1$); both crystal forms contained a single $\alpha_2\beta_2$-tetramer in the asymmetric unit (*9*, *41*). The monoclinic crystals (1 mm × 0.1 mm × 0.2 mm) of the mutant enzyme (D303E-MDH) reported here constitute a fourth crystal type. The space group was shown to be $P2_1$ (a = 101.85 Å, b = 61.02 Å, c = 212.68 Å, and β = 92.83°) and there were two $\alpha_2\beta_2$ MDH tetramers per asymmetric unit. The structure was determined at 3 Å by molecular replacement; after refinement, the final R-factor was 18.7%, with a corresponding free R-factor of 21.7%. The polypeptide chain backbone had continuous electron density for both molecules in the asymmetric unit and well-defined electron density for one molecule of PQQ and one calcium ion in the active site in each α subunit. A summary of data collection parameters and refinement data is given in Table 2.

The D303E mutation had no major effect on the overall structure of MDH. The main chain atoms of WT-MDH and D303E-MDH superimpose with an rms deviation of 0.2 Å for 667 C_α atoms, and the interatomic distances between PQQ and relevant amino acid side chains, in the region of the active site are not markedly different, the greatest difference being 0.34 Å, with 80% being less than 0.2 Å different. The only notable differences result directly from the change of Asp303 in WT-MDH to Glu303 in D303E-MDH (Table 3; Figure 11). In WT-MDH the carboxyl group of Asp303 is too far away to interact with PQQ or Ca^{2+} directly. By contrast, in D303E-MDH a carboxyl group oxygen (OE1) of Glu303 is more than 1 Å closer to the Ca^{2+} ion (2.4 Å), changing the coordination of the Ca^{2+} from hexacoordinate to the more usual heptacoordinate and shifting the Ca^{2+} ion about 0.5 Å in a direction perpendicular to the plane of the PQQ toward the disulfide bridge. The same oxygen atom (OE1) is also located so close to the O5 of PQQ (2.8 Å instead of 4.1 Å) that there must be a hydrogen bond between these oxygen atoms. The most likely explanation is that the PQQ is in the reduced (or semiquinone) form with a hydroxyl on the C5, as seen in the structure of MDH from *M. methylotrophus* (*53*); however, the resolution is not sufficiently high to see whether the C5 atom is in the expected tetrahedral conformation.

DISCUSSION

Asp303 has been proposed previously to be the catalytic base that initiates proton abstraction from the methanol hydroxyl group (*1*, *2*, *6*, *8*) (Figure 2), and it is not surprising that its replacement by the alternative base (glutamate) gave an enzyme (D303E-MDH) which retained some activity. The kinetics with respect to methanol and the activator ammonia, and the deuterium isotope effect were consistent with the overall reaction mechanism being unchanged in the mutant enzyme. The decrease in apparent affinity for methanol in the D303E-MDH (K_m increases from 3 μM to 250 mM) and the decrease in stability of the transition state complex are consistent with the observed changes in the active site region. These include the movement of the Ca^{2+} ion, the new coordination of Glu303 with the Ca^{2+} ion, the replacement of the hydrogen bond with Arg331 with a hydrogen bond to the O5 of PQQ, and the general steric restrictions due to the introduction of the longer side chain of Glu303. Besides hydrophobic interactions, the binding of methanol prior to proton abstraction is presumably by way of a hydrogen bond to the active site base (Asp303), and possibly by coordination to the Ca^{2+} ion which would increase its coordination from 6 to 7. There is an appropriate amount of space to accommodate methanol sufficiently close to the Ca^{2+} ion. It should be noted that if the methanol is able to bind to the

Ca^{2+} ion, then the ammonia base might possibly also bind there which would be consistent with the kinetic data presented in this paper. The decrease in binding energy of methanol in the D303E-MDH is possibly due to poorer binding to the Glu303 and perhaps because it binds more poorly to the Ca^{2+} (giving an octa-coordinated structure). We have also considered the possibility that the methoxide ion is the true substrate for the mutant enzyme as its abundance broadly reflects the very high apparent K_m for methanol, and its binding and entry to the catalytic reaction would be less compromised by the new bonding pattern of Glu303. However, a more detailed analysis is inappropriate in the absence of a structure of the oxidized form of MDH (that is, the form that binds methanol) or of any structure containing bound substrate. Only one such structure has been reported (*5*) but a recent reinterpretation by Mathews and co-workers (*53*) has demonstrated that there is no methanol present and that the PQQ is in the reduced form, with the C5 carrying a hydroxyl group (structure 3 in Figure 2B) which is not an intermediate in the addition−elimination mechanism (Figure 2A). These authors point out that the immediate implication of their observations is that MDH follows the alternative hydride transfer mechanism (Figure 2B), first proposed for MDH (*1*, *2*, *54*), which is in agreement with the mechanism for the related soluble glucose dehydrogenase published recently by Dijkstra and co-workers (*15*−*17*, *55*). This interpretation is consistent with our failure to demonstrate detectable spectroscopic intermediates during the course of the reaction, and our observation that Glu303 is able to make a hydrogen bond with the O5 oxygen of PQQ in D303E-MDH, which would only be possible if there is a hydroxyl in this position.

In the direct hydride transfer mechanism the proton transfer reaction during the tautomerisation process (Figure 2B) is likely to involve a nearby base, probably the same base as catalyses the initial proton abstraction (*1*, *2*, *8*). If this is the case then an oxygen atom of D303 or E303 must be within about 3 Å of the donor (C5 of PQQ) and acceptor (O4 of PQQ) atoms. The distances depicted in Figure 11 and Table 3 demonstrate that this is not the case. The nearby Arg331 is an alternative candidate, with NH2 being within hydrogen bonding distance of O4, but it is probable that the "arm" of the aspartate (or glutamate) side chain is sufficiently flexible for it to carry out both functions; the initial proton abstraction and facilitation of the subsequent tautomerisation of the reduced PQQ.

REFERENCES

1. Anthony, C. (1996) *Biochem. J. 320*, 697−711.
2. Anthony, C. (2000) *Subcell. Biochem. 35*, 73−117.
3. Xia, Z.-X., Dai, W.-W., Xiong, J.-P., Hao, Z.-P., Davidson, V. L., White, S. A., and Mathews, F. S. (1992) *J. Biol. Chem. 267*, 22289−22297.
4. Xia, Z.-X., Dai, W.-W., Zhang, Y.-F., White, S. A., Boyd, G. D., and Mathews, F. S. (1996) *J. Mol. Biol. 259*, 480−501.
5. Xia, Z.-X., He, Y.-N., Dai, W.-W., White, S. A., Boyd, G. D., and Mathews, F. S. (1999) *Biochemistry 38*, 1214−1220.
6. White, S., Boyd, G., Mathews, F. S., Xia, Z.-X., Dai, W.-W., Zhang, Y.-F., and Davidson, V. L. (1993) *Biochemistry 32*, 12955−12958.
7. Blake, C. C. F., Ghosh, M., Harlos, K., Avezoux, A., and Anthony, C. (1994) *Nat. Struct. Biol. 1*, 102−105.
8. Anthony, C., Ghosh, M., and Blake, C. C. F. (1994) *Biochem. J. 304*, 665−674.
9. Ghosh, M., Anthony, C., Harlos, K., Goodwin, M. G., and Blake, C. C. F. (1995) *Structure 3*, 177−187.
10. Anthony, C., and Ghosh, M. (1998) *Prog. Biophys. Mol. Biol. 69*, 1−21.
11. Avezoux, A, Goodwin, M. G., and Anthony, C. (1995) *Biochem. J. 307*, 735−741.
12. Duine, J. A., and Frank, J. (1980) *Biochem. J. 187*, 213-219.
13. Frank, J., Dijkstra, M., Duine, J. A., and Balny, C. (1988) *Eur. J. Biochem. 174*, 331−338.
14. Dijkstra, M., Frank, J., and Duine, J. A. (1989) *Biochem. J. 257*, 87−94.
15. Olsthoorn, A. J. J., and Duine, J. A. (1998) *Biochemistry 37*, 13854−13861.
16. Oubrie, A., Rozeboom, H. J., Kalk, K. H., Olsthoorn, A. J. J., Duine, J. A., and Dijkstra, B. W. (1999) *EMBO J. 18*, 5187−5194.
17. Oubrie, A., and Dijkstra, B. W. (2000) *Protein Sci. 9*, 1265−1273.
18. Anthony, C. (1992) *Biochim. Biophys. Acta 1099*, 1−15.
19. Dales, S. L., and Anthony, C. (1995) *Biochem. J. 312*, 261−265.
20. Chen, L. Y., Durley, R. C. E., Mathews, F. S., and Davidson, V. L. (1994) *Science 264*, 86−90.
21. Read, J., Gill, R., Dales, S. L., Cooper, J. B., Wood, S. P., and Anthony, C. (1999) *Protein Sci. 8*, 1232−1240.
22. Yamada, M., Inbe, H., Tanaka, M., Sumi, K., Matsushita, K., and Adachi, O. (1998) *J. Biol. Chem. 273*, 22021−22027.
23. Elias, M. D., Tanaka, M., Izu, H., Matsushita, K., Adachi, O., Yamada, M. (2000) *J Biol. Chem. 275*, 7321−7326.
24. Yoshida, H., Kojima, K., Witarto, A. B., and Sode, K. (1999) *Protein Eng. 12*, 63−70.
25. Cozier, G. E., Salleh, R. A., and Anthony, C. (1999) *Biochem. J. 340*, 639−647.
26. Cozier, G. E., and Anthony, C. (1995) *Biochem. J. 312*, 679−685.
27. Goodwin, P. M., and Anthony, C. (1998) *Adv. Microb. Physiol. 40*, 1−80.
28. Amaratunga, K., Goodwin, P. M., O'Connor, C. D., and Anthony, C. (1997) *FEMS Microbiol. Lett. 146*, 31−38.
29. Amaratunga, K., Goodwin, P. M., O'Connor, C. D., and Anthony, C. (1997) *FEMS Microbiol. Lett. 150*, 175−177.
30. Nunn, D. N., and Lidstrom, M. E. (1986a) *J. Bacteriol. 166*, 581−590.
31. Nunn, D. N., and Lidstrom, M. E. (1986b) *J. Bacteriol. 166*, 591−597.
32. Sambrook, J., Fritsch, E. F., and Manaiatis, T. (1989) in *Molecular cloning: A laboratory manual*, 2nd ed. Cold Spring Harbor Laboratory Press, New York.
33. Amaratunga, K. (1995) Ph.D. Thesis, University of Southampton, U.K.
34. Dales, S. L. (1995) Ph.D. Thesis, University of Southampton, U.K.
35. Majekodunmi, O. (1997) Ph.D. Thesis, University of Southampton, U.K.
36. Kunkel, T. A. (1985) *Proc. Natl. Acad. Sci. U.S.A.* 82, 488−492.
37. Kunkel, T. A., Roberts, J. D., and Zakour, R. A. (1987) *Methods Enzymol. 154*, 367−382.
38. Day, D. J., and Anthony, C. (1990a) *Methods Enzymol. 188*, 210−216.
39. Day, D. J., and Anthony, C. (1990b) *Methods Enzymol. 188*, 298−303.
40. Goodwin, M. G., and Anthony, C. (1996) *Biochem. J. 318*, 673−679.
41. Ghosh, M., Harlos, K., Blake, C. C. F., Richardson, I., and Anthony, C. (1992) *J. Mol. Biol. 228*, 302−305.
42. Leslie, A. G. W. (1992) in *Joint CCP4 and ESF-EACMB Newsletter on Protein Crystallography No 26*, Daresbury Laboratory, Warrington, U.K.

43. CCP4 (1994) *Acta Crystallogr., Sect. D 50*, 760−763.
44. Matthews, B. W. (1968) *J. Mol. Biol. 33*, 491−497.
45. Vagin, A., and Teplyakov, A. (1997) *J. Appl. Crystallogr. 30*, 1022−1025.
46. Wang, D., Driessen, H. P. C., and Tickle, I. J. (1991) MOLPAC: molecular graphics for studying the packing of protein molecules in the unit cell. *J. Mol. Graph. 9*, 50−52.
47. Brunger, A. T., Adams, P. D., Clore, G. M., DeLano, W. L., Gros, P., Grosse-Kunstleve, R. W., Jiang, J. S., Kuszewski, J., Nilges, M., Pannu, N. S., Read, R. J., Rice, L. M., Simonson, T., and Warren, G. L. (1998) *Acta Crystallogr., Sect. D 54*, 905−921.
48. Brünger, A. T. (1992) *Nature 355*, 472−475.
49. Laskowski, R. A., McArthur, M. W., Moss, D. S., and Thornton, J. M. (1993) *J. Appl. Crystallogr. 26*, 283−291.
50. Moore, G. R., and Pettigrew, G. W. (1990) in *Cytochromes c: Evolutionary, structural and physicochemical aspects*, Springer-Verlag, London.
51. Bullock, W. O., Fernandez, J. M., and Short, J. M. (1987) *Biotechniques 5*, 376−378.
52. Harris, T. K., and Davidson, V. L. (1994) *Biochem. J. 300*, 175−182.
53. Zheng, Y.-J., Xia, Z.-X., Chen, Z.-W., Mathews, F. S., and Bruice, T. C. (2001) *PNAS 98*, 432−434.
54. Anthony, C. (1993) In *Principles and applications of quinoproteins* (Davidson, V. L., Ed.) pp 17−45, Marcel Dekker, New York.
55. Dewanti, A. R., and Duine, J. A. (2000) *Biochemistry 39*, 9384−9392.

BI002932L